Received: 10 August 2018 | Accepted: 2 January 2019

DOI: 10.1002/hyp.13397

RESEARCH ARTICLE

WILEY

On the role of spatial resolution on snow estimates using a process-based snow model across a range of climatology and elevation

Mohammad M. Sohrabi[1] | Daniele Tonina[2] | Rohan Benjankar[3] | Mukesh Kumar[4] | Patrick Kormos[5] | Danny Marks[5] | Charlie Luce[6]

[1] Sierra Nevada Research Institute, UC Water, University of California, Merced, Merced, California, USA

[2] Center for Ecohydraulics Research, University of Idaho, Boise, Idaho, USA

[3] Department of Civil Engineering, Southern Illinois University Edwardsville, Edwardsville, Illinois, USA

[4] Department of Civil, Construction and Environmental Engineering, University of Alabama, Tuscaloosa, Alabama, USA

[5] USDA-ARS Northwest Watershed Research Center, Boise, Idaho, USA

[6] U.S. Forest Service, Rocky Mountain Research Station, Boise, Idaho, USA

Correspondence
Mohammad M. Sohrabi, Sierra Nevada Research Institute, UC Water, University of California, Merced, 5200 Lake Street, Merced, CA 95340.
Email: sohrabi@uidaho.edu; msohrabi2@ucmerced.edu; s0hrabi@yahoo.com

Funding information
Idaho's IGEM programme; Murdock Charitable Trust; National Science Foundation, Grant/Award Numbers: EAR-1454983, EAR-1331846 and CNS-1229766; Bureau of Reclamation, Grant/Award Number: RI2APJ 1025

Abstract

Hydrological processes in mountainous settings depend on snow distribution, whose prediction accuracy is a function of model spatial scale. Although model accuracy is expected to improve with finer spatial resolution, an increase in resolution comes with modelling costs related to increased computational time and greater input data and parameter information. This computational and data collection expense is still a limiting factor for many large watersheds. Thus, this work's main objective is to question which physical processes lead to loss in model accuracy with regard to input spatial resolution under different climatic conditions and elevation ranges. To address this objective, a spatially distributed snow model, *iSnobal*, was run with inputs distributed at 50-m —our benchmark for comparison—and 100-m resolutions and with aggregated (averaged from the fine to the large resolution) inputs from the 50-m model to 100-, 250-, 500-, and 750-m resolution for wet, average, and dry years over the Upper Boise River Basin (6,963 km^2), which spans four elevation bands: rain dominated, rain–snow transition, and snow dominated below treeline and above treeline. Residuals, defined as differences between values quantified with high resolution (>50 m) models minus the benchmark model (50 m), of simulated snow-covered area (SCA) and snow water equivalent (SWE) were generally slight in the aggregated scenarios. This was due to transferring the effects of topography on meteorological variables from the 50-m model to the coarser scales through aggregation. Residuals in SCA and SWE in the distributed 100-m simulation were greater than those of the aggregated 750 m. Topographic features such as slope and aspect were simplified, and their gradient was reduced due to coarsening the topography from the 50- to 100-m resolution. Therefore, solar radiation was overestimated, and snow drifting was modified and caused substantial SCA and SWE underestimation in the distributed 100-m model relative to the 50-m model. Large residuals were observed in the wet year and at the highest elevation band when and where snow mass was large. These results support that model accuracy is substantially reduced with model scales coarser than 50 m.

KEYWORDS

alpine treeline, model accuracy, model evaluation, mountainous regions, physics-based snow modelling, rain–snow transition, spatial resolution

1 | INTRODUCTION

As physically based models are increasingly adopted for use in operational river basin forecasting and climate change projection (Gupta, Sorooshian, & Yapo, 1998; Tobin & Bennett, 2017), questions about the importance of fine-scale physical heterogeneity in snowpack representation in models are becoming priorities (Clark et al., 2016). Accumulation and ablation of snow is critical for hydrological cycles and ecological systems in mountainous settings (Homan, Luce, McNamara, & Glenn, 2010; Kumar, Wang, & Link, 2012; Nitaa et al., 2014; Raleigh & Lundquist, 2012). Spatio-temporal distribution of these water releases is critical for hydrological studies, as it influences a swath of hydrologic states and fluxes such as soil moisture (Kormos, Marks, McNamara, et al., 2014; Liston & Elder, 2006), groundwater recharge (Kormos, Marks, Williams, et al., 2014; Kumar et al., 2012), evapotranspiration (Wang, Kumar, & Marks, 2013), and run-off and streamflow generation (Garen & Marks, 2005; Weill et al., 2013). In addition, the water supply that supports ecosystem sustainability depends on the spatio-temporal distribution of snow accumulation and ablation with respect to tree growth and mortality. Spring and early summer air temperatures and soil moisture distribution are fundamental controls for vegetation pattern (Darmody, Thorn, Shlyter, & Dixon, 2004; Molotch & Bales, 2005; Sensoy, Sorman, Tekeli, Sorman, & Garen, 2006; Torp, 2010). Soil microbial activity during winter may continue during extreme winter temperatures due to snow cover (Schimel, Bilbrough, & Welker, 2004), which insulates the soil from very low air temperatures due to low thermal conductivity of snow (Luce & Tarboton, 2010; Sturm, Holmgren, König, & Morris, 1997). Contribution of snow melt to discharge prevents stream temperature from following the increasing trend in air temperatures in late spring and early summer (Luce et al., 2014; Sohrabi, Benjankar, Tonina, Wenger, & Isaak, 2017). As a result, stream temperature, which is an important element for aquatic ecosystems, is influenced by spatio-temporal distribution of melt (Cristea & Burges, 2010; Gu, McCutcheon, & Chen, 1999; Webb, Clack, & Walling, 2003).

A high-level question is whether the spatial details of snow accumulation and melt (their spatial heterogeneity) in terms of mass and energy balances are important with respect to its average behaviour, characterized by homogeneous values spatially averaged at the higher spatial distribution, or whether they can be extracted for later use after a coarse-resolution model is applied to obtain "average" behaviour. This fits within a broad class of questions about the effects of model computational choices on model output (Clark et al., 2015; Mizukami et al., 2014). A specific pair of choices for a snow model revolve around (a) how coarse the snow modelling resolution can be, even if weather (e.g., precipitation, radiation, temperature, and humidity) can be estimated at fine scales, and (b) how coarsely the weather information can be averaged. These questions have practical relevance in terms of data needs and run times, the latter point being critical for operational forecasts. However, we should also recognize that there is a great base of results from low-resolution modelling, and it is worth understanding the biases that may be inherent in using such information by examining the scale dependence of different processes within the model and how these biases might change in different portions of a mountain landscape, as we range from foothills to alpine settings.

Here, we first examine the sensitivity to degrading snowpack model support scale (Blöschl & Sivapalan, 1995) by spatially (but not temporally) averaging weather input data calculated at fine scales to successively larger scales and running the snowmelt model under the averaged inputs. We follow this up by degrading the resolution at which the weather calculations are made and then computing the snowpack evolution under the degraded resolution weather inputs. Although much weather information is calculated as a coarse surface from widely spaced instruments, some local information based on elevation, aspect, slope, and wind sheltering is much more local in nature. By examining the details of differences and supplementing with additional numerical modelling experiments, we sought to better understand which processes and fluxes were most compromised in different environments to provide guidance for improving model performance.

2 | BACKGROUND

Others have looked at scale issues with models (Bloschl, 1999; Kirnbauer, Blöschl, & Gutknecht, 1994; Luce, Tarboton, & Cooley, 1998; Pohl & Marsh, 2006; Tarboton, Blöschl, Cooley, Kirnbauer, & Luce, 2001). Topographic features and/or spatial vegetation changes influence the snow distribution (Winstral, Marks, & Gurney, 2014) by modifying meteorological variables such as radiation, wind, and precipitation (Elder, Dozier, & Michaelse, 1991; Marks, Domingo, Susong, & Link, 1999; Trujillo, Rami, & Elder, 2007). Although heterogeneous snow accumulation is mainly due to spatial variability of precipitation and redistribution of snow (Trujillo et al., 2007), spatial variations in energy fluxes may cause heterogeneous snow ablation (Pohl & Marsh, 2006). At watershed scale, precipitation distribution often varies with elevation (Winstral, Marks, & Gurney, 2013). Even if precipitation pattern was uniform over a watershed, snow accumulation could be complex due to wind heterogeneity (Elder et al., 1991; Luce, Tarboton, & Cooley, 1999; Winstral & Marks, 2002), which leads to preferred deposition of snow in sheltered areas (Liston, 2004; Winstral, Marks, & Gurney, 2009). Variations in slope and aspect cause spatial variations in radiation, especially on sunny days, playing a key role in snow ablation heterogeneity (Keller, Goyette, & Beniston, 2005; Pohl & Marsh, 2006). On warm and cloudy days, spatial variation in longwave emissions from trees (Seyednasrollah & Kumar, 2014; Seyednasrollah, Kumar, & Link, 2013) and heterogeneity in turbulent energy caused by spatial disparity in air temperature, vapour pressure, and wind speed may lead to snow ablation heterogeneity (Marks, Winstral, Reba, Pomeroy, & Kumar, 2013; Pohl, Marsh, & Liston, 2006). Similarly, spatial variations of soil temperatures are especially important for snowpack development in lower elevation terrain bands.

Neglecting spatial variations of aforementioned meteorological variables and energy fluxes is likely to impact estimation of snow cover properties. The extent of this impact may vary in different elevation ranges and climate conditions. In rain-dominated and rain–snow transition bands, where precipitation can fall as either rain or snow, precipitation phase may be misidentified due to estimated patterns of dew point or wet-bulb temperature (Beniston, 2012). This can cause inaccurate estimation of snow mass and advected heat from

precipitation to the snow cover. In snow-dominated bands, it is critical to capture small scale variations in snow drifting and energy exchanges at the snow–air interface (Luce et al., 1998). Estimation of the energy exchange between snow and the atmosphere can be less reliable when topography- and vegetation-induced spatial disparity in solar radiation and turbulent energy is neglected. Spatial disparity in meteorological variables is also likely to vary between years that have different climate conditions. For example, in a wet year, spatial disparity in dew point temperature and energy fluxes is on average less pronounced due to high humidity and large number of cloudy days (Rohli & Vega, 2008). In contrast, in a dry year, spatial variability in these variables is pronounced. These examples suggest that the effect of model scale on prediction accuracy is likely to vary across elevation bands and years with characteristically different climatology.

To accurately account for heterogeneity in snow accumulation and ablation, a model scale that is able to capture process scale (natural) variations is required (Bloschl, 1999). For instance, process scale (correlation length) is small in regions where snow water equivalent (SWE) changes substantially over small distances. Therefore, in order to capture variations in SWE, the model scale needs to be finer than the process scale or the model must have a tool to consider subgrid variability (Liston, 2004; Luce et al., 1999; Luce & Tarboton, 2004; Meromy, Molotch, Link, Fassnacht, & Rice, 2013; Nitaa et al., 2014; Niu & Yang, 2007).

To identify an appropriate spatial scale for snow modelling, it is important to analyse the effects of scaling on estimation of snow accumulation and ablation. Scaling effect on prediction of snow accumulation and ablation can be evaluated using three approaches (Bloschl, 1999): (a) a spectral analysis; (b) a variogram analysis; and (c) analysing changes in the average value of a snow variable, that is, SWE, over an area by coarsening the measurement resolution or the model scale. All these three approaches lead to the same result for linear processes. However, for non-linear processes, the third approach may yield different results than the first two approaches (Bloschl, 1999). This is due to the impact of scale change on the mean value of a variable over an area. Estimation of SWE is a non-linear process, because SWE estimation relies on meteorological variables with topography-induced spatial variation, that is, solar radiation and snow drifting (Bloschl, 1999; Hopkinson, Chasmer, Munro, & Demuth, 2010). Topographic features, such as slope, aspect, and sky view factor, change as model scale changes. As a result, average values of SWE over a basin estimated using different model scales are not necessary the same, even though physics-based snow models conserve mass and energy to estimate SWE.

Scaling impacts on snow cover properties have been investigated in previous studies using the stated three approaches. Deems, Fassnacht, and Elder (2006) and Trujillo et al. (2007) analysed scaling effect on snow depth from LIDAR data at a couple of Colorado catchments using variogram and spectral analyses, respectively. They reported that scale breaks (correlation length) of snow depth ranged from 15 to 40 m. They also found that scaling behaviour of snow depth depends on spatial distribution of vegetation height and wind. Furthermore, they concluded that scaling characteristics of snow depth is controlled by spatial distribution of vegetation height in forested regions where interception is the dominant factor for snow distribution. However, in nonforested or sparse forested regions, where wind is responsible for snow redistribution, scaling characteristics of snow depth is controlled by wind. Winstral et al. (2014) analysed sensitivity of basin-averaged surface water input (SWI) to the model scale and used spatial resolution of 10 to 1,500 m for inputs to run a distributed physics-based snow model (*iSnobal*) over a small watershed (6 km^2). They observed that simulated basin-averaged SWI using 100-m resolution of the inputs was very similar to that of 10-m resolution with less than 4% bias. However, they concluded that due to small drainage area of the studied watershed, selecting the appropriate model scale for other watersheds requires further analyses related to the watershed of interest.

There is no optimum model scale for snow modelling, because in practice, a grid size is selected by considering data availability, modelling costs and required resolution, and/or accuracy of predictions for the specific question being investigated (Bloschl, 1999; Winstral et al., 2014). In distributed snow models that require distributed inputs of forcing, the use of a fine model scale substantially increases the modelling costs, such as runtime and storage space. Increase in the modelling costs is mainly due to spatially distributing forcing inputs rather than running snow models (Winstral et al., 2014). On the other hand, using a coarse model scale neglects small scale variations, which reduces prediction accuracy. The extent of the reduction in model accuracy, vis-à-vis if the setting is snow dominated versus rain–snow transition zone or depending on if the year is wet or dry, remains unknown. As prior studies on scaling of snow states were either limited for a short period of a snow season or small spatial extent, they could not fill this knowledge gap. In addition, the majority of the previous studies explored the effects of model scale on prediction accuracy by aggregating inputs, basically averaging the fine spatial distribution within a coarse grid, from a fine resolution to obtain coarse resolution. This may result in implicit transfer of information from inputs with a fine resolution to those with coarse resolutions. Notably, the aggregated inputs do not account for the loss in prediction accuracy due to coarsening of the digital elevation model (DEM), and its effect on estimation of meteorological forcings.

The objective of this work is to understand the errors associated with coarsening (both aggregated and coarse inputs) of the model scale and its consequent effects on estimation of meteorological forcings. Comparing coarsening as aggregated inputs and coarse spatial input will help to understand the implicit transfer of information from fine to coarse grid due to aggregated inputs. We also seek to understand how the errors vary for a range of climatic and topographic conditions. To address these objectives, we (a) quantify the impact of model scale on snow model response by analysing snow-covered area (SCA) and SWE, (b) assess the role of annual precipitation amount on the estimation accuracy, and (c) identify the elevation range where estimation accuracy is most sensitive to model scale.

3 | STUDY AREA AND DATA

The study area is the portion of the Boise River Basin (BRB; Idaho, USA), upstream of the Lucky Peak Dam, with drainage area of

6,963 km^2 (Figure 1). This portion of the BRB has three reservoirs, including Lucky Peak, Arrow Rock, and Anderson Ranch Dams, which provide protection from flooding and water for agricultural and urban uses. Vegetation cover of the BRB is mainly coniferous forest (41%) and shrubland (35%), and the rest of the BRB is covered with bare rock, grass, deciduous forest, or burned/harvested forest. Elevation in the BRB ranges from 841 to 3,186 m and extends from rain- to snow-dominated regions. Average annual precipitation in the basin varies from about 500 mm at low elevations to approximately 1,500 mm at high elevations.

There are 18 weather and SNOTEL stations in or near BRB that measure hourly meteorological variables, including precipitation (p), air temperature (t), relative humidity (rh), solar radiation (sr), and wind (w; Figure 1 and Table 1). Precipitation and temperature are measured at all the stations, whereas relative humidity, solar radiation, and wind are available at five, six, and nine of these stations, respectively. Ten of these 18 stations are SNOTEL sites that are operated by the Natural Resources Conservation Service, and the rest of the stations are weather stations that are operated either by the Bureau of Land Management and U.S. Department of Agriculture Forrest Service (five stations) or by the Bureau of Reclamation (three stations).

4 | METHODOLOGY

4.1 | Snow model: *iSnobal*

Snobal is a physics-based snow model that conserves both mass and energy at a point (Marks, 1988). Spatial (image) version of *Snobal*, *iSnobal*, was developed by Marks et al. (1999) and uses the same set of equations as *Snobal* to calculate mass and energy flux exchanges at each grid cell. The model uses a two-layer representation of the snow cover with a 0.25-mm fixed-thickness top layer and a bottom layer with the rest of the snowpack. Calculation of water exchanges between snow and the atmosphere, such as evaporation, condensation, and sublimation, is conducted only in the top layer. However, computation of energy exchanges are performed in both layers at each time step for each grid cell using the following energy balance equation (Equation (1); Marks et al., 1999):

$$\Delta Q = R_n + H + L_v E + G + M \quad (1)$$

where ΔQ (W m^{-2}) is the net snow cover energy exchange that depends on changes in net radiation (R_n), sensible heat (H), latent heat ($L_v E$), conduction (G), and advection (M) energies (all units of W m^{-2}). L_v (W m^{-2} kg^{-1}) indicates specific latent heat of vaporization of water, and E (kg) represents mass of water that undergoes phase change. An increase in the net snow cover energy exchange causes a decrease in the cold content, which is the energy required to bring the snow cover temperature to 0°C. Melt is calculated in both layers and occurs once the cold content reaches 0°C. Estimated melt in the model consists of both melt and rain on snow, and it drains out when total liquid water content in snowpack is higher than a specified threshold. Melt that drains out is surface water input (SWI).

4.2 | Spatial distribution of meteorological data

Distributed meteorological inputs such as precipitation, air temperature, vapour pressure, solar radiation, and wind speed are required to force *iSnobal*. Details about the spatial interpolation methodology for meteorological variables were described in our previous work (Sohrabi, 2016; Sohrabi et al., 2018), and the following is a brief description about the method used. Inputs were spatially distributed using interpolation detrended elevation (vertical) and distance

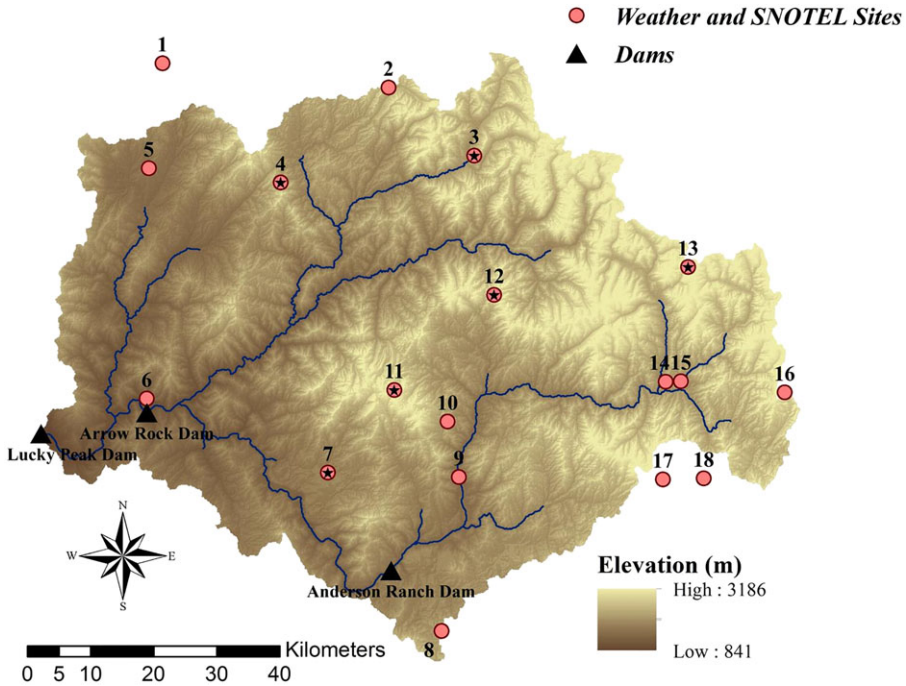

FIGURE 1 Digital elevation map of the Boise River Basin showing the location of weather and SNOTEL sites. Black stars indicate SNOTEL sites with snow water equivalent measurements, which were used in the evaluation of model performance

TABLE 1 Detailed information of the stations

No.	Station name	Latitude (Decimal °)	Longitude (Decimal °)	Elevation (m)	Variables measured	Operated by
1	LITTLE ANDERSON	44.09	−115.88	1,389	p, t, rh, sr, w	BLM & FS
2	JACKSON PEAK	44.05	−115.44	2,155	p, t, w, SWE	NRCS
3	GRAHAM GUARD STA.	43.95	−115.27	1,734	p, t, w, SWE	NRCS
4	MORES CREEK SUMMIT	43.93	−115.67	1,859	p, t, SWE	NRCS
5	TOWN CREEK	43.94	−115.91	1,415	p, t, rh, sr, w	BLM & FS
6	ARROWROCK DAM	43.61	−115.92	998	p, t	BR
7	PRAIRIE	43.50	−115.57	1,463	p, t, SWE	NRCS
8	CAMAS CREEK DIVIDE	43.27	−115.35	1,740	p, t, SWE	NRCS
9	SOUTH FORK BOISE	43.49	−115.31	1,286	p, t	BR
10	WAGONTOWN	43.57	−115.33	1,881	p, t, rh, sr, w	BLM & FS
11	TRINITY MOUNTAIN	43.63	−115.44	2,368	p, t, SWE	NRCS
12	ATLANTA SUMMIT	43.76	−115.24	2,310	p, t, sr, w, SWE	NRCS
13	VIENNA MINE	43.80	−114.85	2,731	p, t, w, SWE	NRCS
14	FLECK SUMMIT	43.62	−114.90	2,164	p, t, rh, sr, w	BLM & FS
15	BIG SMOKEY RANGER	43.62	−114.87	1,706	p, t	BR
16	DOLLARHIDE SUMMIT	43.60	−114.67	2,566	p, t, SWE	NRCS
17	SOLDIER MOUNTAIN PEAK	43.48	−114.91	2,904	p, t, rh, w	BLM & FS
18	SOLDIER R.S.	43.48	−114.83	1,749	p, t, SWE	NRCS

Note. Variable abbreviations. p: precipitation; t: air temperature; rh: relative humidity; sr: solar radiation; w: wind speed and direction; SWE: snow water equivalent. Abbreviations for institutes operate the stations. BLM & FS: Bureau of Land Management and U.S. Department of Agriculture (USDA) Forrest Service, respectively; NRCS: Natural Resources Conservation Service; BR: Bureau of reclamation.

(horizontal) Kriging method (Garen & Marks, 2005). Air temperature versus elevation trends were constrained to zero or a negative value because air temperature decreases as elevation increases. However, we did not constrain the variation of relative humidity with elevation. The distributed relative humidity and air temperature was then used to compute dew point temperature and vapour pressure. Dew point temperatures were used to identify precipitation phase (Garen & Marks, 2005). Wind speed and direction were distributed using a detrended elevation and distance-based Kriging method. Wind speed of a cell, then, was adjusted using Winstral, Elder, and Davis (2002) algorithm. In this algorithm, topographically wind exposed and sheltered cells are identified using maximum upwind slope (s_x). At exposed cells, negative s_x, wind speed is increased due to vertical flow constriction, whereas wind speed is decreased at topographically sheltered cells, positive s_x, due to expansion of flow (Winstral et al., 2002). Analogous to wind speeds, precipitation was first distributed using a detrended elevation and distance-based Kriging method. Precipitation versus elevation trends were constrained to zero or a positive value as precipitation generally increases with elevation in this region (Garen & Marks, 2005). Wind-induced snow drifting was, then, calculated using upwind slope break (s_b) and wind speed (Winstral et al., 2002, 2013, 2014). Snow is eroded at exposed cells once wind speed is high. The transported snow particles from these cells are, then, deposited at sheltered cells where wind speed is low. Solar radiation was distributed using a detrended elevation and distance-based Kriging method. The distributed solar radiation was then corrected for solar angle, shading, vegetation, and albedo (Link & Marks, 1999; Susong, Marks, & Garen, 1999). Snow albedo was adjusted to consider snow aging due to dust and organic debris exposure (Garen & Marks, 2005). Distributed thermal radiation was computed for clear sky based on the distributed air temperature and vapour pressure and elevation and sky view factor. The calculated thermal radiation was then adjusted given cloud cover and vegetation (Link & Marks, 1999).

4.3 | Scenarios

To evaluate the effects of scaling on estimation of SCA and SWE, *iSnobal* was run for five different grid sizes (scale) of inputs, including 50 (50 m (d)), 100 (100 m (a)), 250 (250 m (a)), 500 (500 m (a)), and 750 m (750 m (a)). We distributed the inputs at 50-m resolution, and the distributed inputs were then aggregated to obtain 100- to 750-m resolutions of inputs, which are hereafter referred as aggregated scenarios and are indicated as 100 (a) to 750 m (a). Aggregated scenarios used in this work are similar to those used in Winstral et al. (2014). Resolutions coarser than 750 m were not used as Winstral et al. (2014) identified those scales as inappropriate for resolving watershed scale-based heterogeneities. In addition to the aggregated scenarios, we ran *iSnobal* using inputs that were distributed at 100-m resolution, hereafter referred as 100-m (d) scenario. This scenario allows evaluation of the role of coarsening of DEM on meteorological forcings and eventually on the estimation accuracy of snow states.

Hourly time step of inputs was used, and model runs were performed for the entire water years (WY), which start on October 1 of the previous year and end on September 30 of the current year. Each scenario was run for a wet (WY2006—359 mm), average (WY2010—325 mm), and dry year (WY2007—209 mm) to understand the sensitivity of model scale for a range of climatic conditions. These years were identified from the period of 1950–2010 using four different drought indices at Boise Airport station, which has a lower elevation than BRB (Sohrabi, Ryu, Abatzoglou, & Tracy, 2013, 2015).

4.4 | Model performance evaluation and analyses

SWE estimation at a 50-m grid scale has already been validated for wet, average, and dry years (Sohrabi, 2016; Sohrabi et al., 2018) using measured SWE at six out of the 10 SNOTEL sites located inside BRB: Prairie, Graham Guard, Mores Creek Summit, Atlanta Summit, Trinity Mountain, and Vienna Mine (Figure 1). Average Nash–Sutcliffe coefficient of 0.76 and ratio of root mean square error and observation standard deviation ratio of 0.42 over all sites and years. Nash–Sutcliffe coefficient and root mean square error and observation standard deviation ratio values were generally larger than 0.75 and lower than 0.5, indicating reliable estimates (Moriasi et al., 2007). For snow states that are a direct consequence of non-linear processes such as SCA and SWE, an appropriate approach to understand scaling effects is to analyse changes in the mean values of these variables over an area as scale changes (Bloschl, 1999). To do this, estimated daily time series of SCA and SWE from all the scenarios were divided into four elevation bands (Table 2). At the rain–snow transition region (E2), where precipitation can fall as either rain or snow, precipitation phase is very sensitive to changes of dew point temperature (Beniston, 2012; Marks et al., 2013). Whereas Kormos, Marks, McNamara, et al. (2014) and Kormos, Marks, Williams, et al. (2014) defined E2 between 1,500 and 1,800 m for the Pacific Northwest, USA, E2 elevation range is wider for the BRB and covers the regions from 1,400- to 1,900-m elevations. The rain- (E1) and snow-dominated (E3) regions are below and above E2, respectively. Alpine treeline (E4) indicates elevation above which trees cannot grow because of low air temperatures and long snow cover duration. E4 in the BRB includes regions that have elevations greater than 2,400 m (Korner, 1998).

Modelled SWE was spatially averaged over each elevation band. SCA represents percent of the area covered with snow, which was calculated by dividing the number of cells with SWE greater than 0 over the total number of cells in each elevation band. The spatially averaged SWE ($\overline{SWE}_{i,j}(t)$) and snow cover area ($SCA_{i,\ j}(t)$) for the i-th band (E1, E2, E3, and E4) with area, A_i, and the j-th scenario, such as 50 (d), 100 (d), 100 (a), 250 (a), 500 (a), and 750 m (a), are computed as follows:

$$\overline{SWE}_{i,j}(t) = \frac{1}{A_i}\int_0^{A_i} SWE_{i,j}(t,a)\,da, \quad \text{with } i = E1 - E4 \text{ and } j = 50\text{d}, 100\text{d}, 100\text{a}, 250\text{a}, 500\text{a}, 750\text{a}, \tag{2}$$

TABLE 2 Elevation bands

Bands	Elevation (m)	Description	% of grid cells	% of total watershed SWE
E1	≤1,400	Rain dominated	16	7.4
E2	>1,400 and ≤1,900	Rain–snow transition	44	21.6
E3	>1,900 and ≤2,400	Snow dominated	28	30.8
E4	>2,400	Alpine treeline	12	40.2

Note. SWE: snow water equivalent.

$$SCA_{i,j}(t) = \frac{100}{A_i}\int_0^{A_i} SC_{i,j}(t,a)\,da \text{ and } \begin{cases} SC_{i,j}(t,a) = 1 & SWE_{i,j}(t,a) > 0 \\ SC_{i,j}(t,a) = 0 & SWE_{i,j}(t,a) = 0 \end{cases}, \tag{3}$$

where $SWE_{i,\ j}(t,a)$ and $SC_{i,\ j}(t,a)$ are the SWE and snow cover index, respectively, for each cell of area a at time t. The spatially averaged residual of SWE and SCA for each band, which was applied for visualizing the results, was computed as follows:

$$\text{Res}_{i,j}(t) = SV_{i,j}(t) - SV_{i,50m}(t), \quad \text{with } i = E1 - E4 \text{ and } j = 100\text{d}, 100\text{a}, 250\text{a}, 500\text{a}, 750\text{a}, \tag{4}$$

where $SV_{i,j}$ stands for $\overline{SWE}_{i,j}(t)$ or $SCA_{i,\ j}(t)$ for j-th scenario. To present residuals in SWE in percentage, the residuals were divided by the mean of the estimated SWE from the 50 m (d) for a given snow season. Effect of scaling on the estimated snow variables for each band was quantified using mean absolute error (MAE). In our case, increase in value of MAE indicates reduction in prediction accuracy. MAE is computed as follows (Moriasi et al., 2007):

$$MAE_{i,j} = \frac{1}{T}\int^{T} \left|SV_{i,j}(t) - SV_{i,50m}(t)\right| dt, \quad \text{with } i = E1 - E4 \text{ and } j = 100\text{d}, 100\text{a}, 250\text{a}, 500\text{a}, 750\text{a}, \tag{5}$$

where T indicates the period of time that MAE is computed. MAE was calculated for the entire snow season (total MAE), accumulation (rising limb [RL]), and ablation (falling limb [FL]) periods at each band. RL begins as snow cover forms and terminates when SWE reaches its peak. FL begins after SWE peak occurs and continues to the time snow ablates completely.

5 | RESULTS AND DISCUSSION

5.1 | Effects of spatial resolution on the model performance

5.1.1 | Snow cover area

Aggregation scenarios

Residuals in the aggregated scenarios increased from less than 2.0% for the 100-m (a) scenario to as large as 17.6% (Figure 2) for the 750-m (a) scenario. Total MAE reduced with the increase in elevation from rain dominated to snow dominated above the treeline (Table 3). The largest MAE for RL and FL were obtained for the 750-m (a) scenario. As elevation increased, MAE decreased for the accumulation period (RL), but MAE increased for the ablation period (FL). Residuals in RL were generally positive, representing overestimation of SCA in the aggregated scenarios relative to the 50-m (d) scenario. In FL, residuals were positive at the beginning of ablation periods but were negative subsequently. Total MAE was largest during the average year and lowest in the wet year for all the aggregated scenarios and elevation bands (Table 3). MAE for RL and FL was larger in the wet year, except in E3 and E4, where dry year had the largest MAE for RL. Neglecting spatial variability of meteorological inputs was responsible for these residuals in the aggregated scenarios. The residuals increased as spatial resolution of the aggregated scenarios increased,

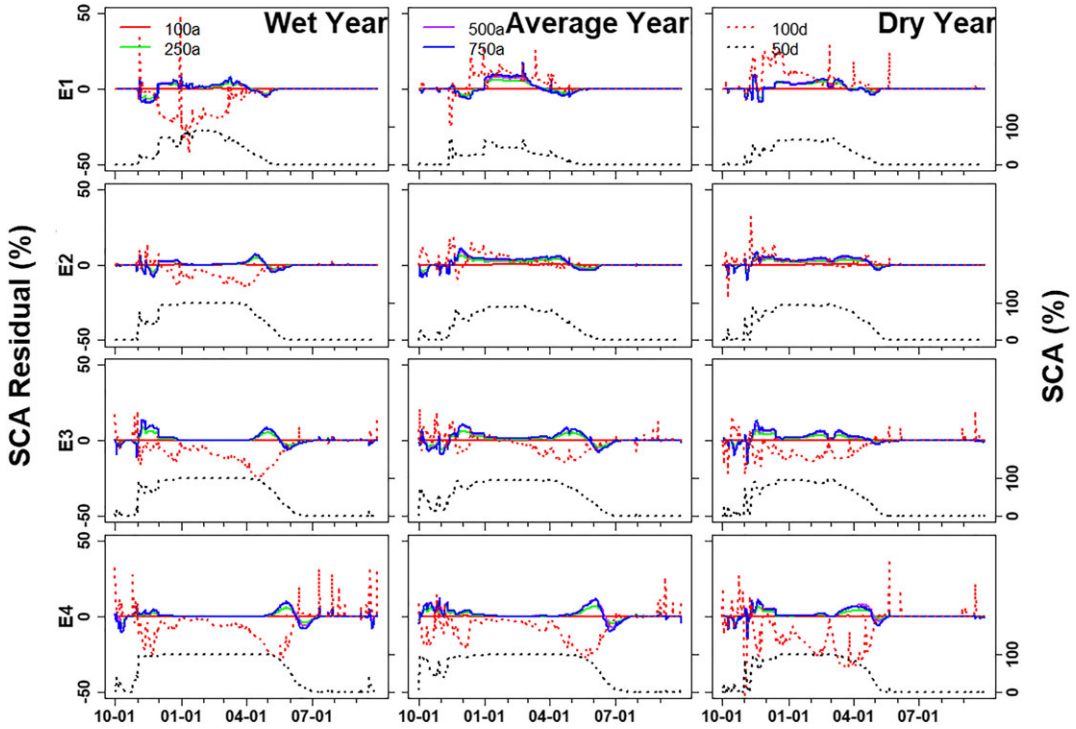

FIGURE 2 Aggregated estimated snow-covered area (SCA) over four climatic regions represented by elevation bands. Dotted lines show the 50-m (d) and 100-m (d) scenarios, and solid lines indicate the aggregated scenarios (100 m (a) through 750 m (a)). The primary Y (left) axis shows residuals between the estimated SCA generated from all the scenarios compared with that of the 50-m (d) scenario. The secondary Y (right) axis shows the estimated SCA from the 50-m (d) scenario

because larger variability of meteorological inputs was lost as spatial resolution of inputs increased.

Distribution scenario

Residuals in the 100-m (d) scenario were even larger than those observed in the 750-m (a) scenario. Maximum residual of 48.7% was observed in the 100 m (d), whereas residuals of the 750 m (a) did not exceed 17.6%. Similar to the aggregated scenarios, MAE generally decreased with increasing elevation from E1 to E4 during RL but increased during FL. Residuals were positive in E1 and E2, except in the wet year that had negative residuals in these bands. Residuals were negative in E3 and E4 for all years. The wet year had large residuals (up to 48.7%) in E1 and E2, but large residuals in E3 and E4 were observed in the dry year. The large difference between the estimated SCA from the 50-m (d) and 100-m (a) simulations and that of the 100-m (d) simulation indicate the need to consider effects of topographic variability on meteorological inputs. Notably, the aggregation of meteorological inputs from 50 to 100 m in 100-m (a) simulation implicitly carries added information and does not truly represent the loss in accuracy due to coarsening of model grid. The 100-m (d) simulation uses a meteorological forcing that has been generated using a 100-m resolution DEM and hence is suited to capture the loss in snow model accuracy with coarsening of the model grid.

5.1.2 | Snow water equivalent

Aggregation scenarios

Similar to SCA, SWE residuals increased with coarsening in the aggregated scenarios. The 50-m (d) and 100-m (a) simulations were similar with total MAE and residuals being less than 0.5 mm and 0.6%, respectively. The 750-m (a) simulation, however, showed a total MAE and residual that were as large as 7.7 mm and 40% (40.8 mm), respectively. Residuals and total MAE were low in E2 with an average residual of 3.7% over all the years. Residuals and total MAE generally increased with elevation from E2 to E4 (Figure 3 and Table 4). The largest residuals were in E1 with an average residual of 11.6% (maximum residual of 10.6 mm) over all the years, whereas the largest total MAE was in E4, which was due to the larger mean SWE in E4 than E1. Residuals were negligible and generally negative during RL, except in E4 whose residuals were generally positive. However, they were large during FL and were more pronounced in E3 and E4 (maximum residual of 40.8 mm) than in E1 and E2 (maximum residual of 19.4 mm). Similar to the SCA results, residuals were positive in the beginning of FL but became negative subsequently. Residuals were larger in the average year with an average residual of 6.8% (maximum residual of 37.5 mm) over all the elevation bands than those of the wet and dry years with average residuals of 4.9% (maximum residual of 40.8 mm) and 4.3% (maximum residual of 15 mm), respectively. As spatial resolution increased in the aggregated scenarios, larger variability in meteorological inputs neglected and caused larger SWE residuals, particularly in years and elevation bands when and where meteorological inputs variation and snow mass were large.

Distribution scenario

Residuals for the 100-m (d) scenario were as large as 66% (117.2 mm) and thus substantially larger than those in the 750 m (a; Figure 3 and Table 4). Residuals were larger in E1 than E2, but total MAE was slightly larger in E2 than E1. Residuals and total MAE increased with

TABLE 3 Mean absolute error (MAE) for snow-covered area (%) in each band for the rising limb, falling limb, and total snow accumulation–ablation cycle

Bands	MAE (%)	100a	250a	500a	750a	100d
E1	RL (Wet|Average| Dry)	0.1|0.1| 0.1	2.9|3.8| 3.1	3.7|5.3| 4.0	3.9|5.9| 3.9	15.3|9.2| 11.9
	FL (Wet|Average| Dry)	0.1|0.1| 0.1	1.5|1.7| 1.4	2.0|2.4| 2.0	2.3|2.5| 2.3	2.8|3.9| 2.2
	Total (Wet|Average| Dry)	0.1|0.1| 0.1	2.5|2.9| 2.5	3.2|4.0| 3.3	3.4|4.5|3.3	11.5|6.9| 8.4
E2	RL (Wet|Average| Dry)	0.0|0.0| 0.0	1.0|2.5| 2.2	1.3|3.7| 3.0	1.4|4.1| 3.5	6.2|4.6| 3.0
	FL (Wet|Average| Dry)	0.0|0.0| 0.0	2.1|1.9| 2.1	2.9|2.7| 2.9	3.1|3.0| 3.2	4.7|1.0| 1.5
	Total (Wet|Average| Dry)	0.0|0.0| 0.0	1.3|2.4| 2.2	1.8|3.4| 3.0	2.0|3.8| 3.4	5.7|2.4| 2.5
E3	RL (Wet|Average| Dry)	0.0|0.0| 0.0	1.4|2.3| 2.6	2.0|3.3| 3.8	2.1|3.6| 4.4	7.9|4.4| 8.6
	FL (Wet|Average| Dry)	0.0|0.0| 0.0	2.2|2.9| 1.3	3.2|4.3| 1.9	3.3|4.5| 2.1	10.4|6.6| 4.5
	Total (Wet|Average| Dry)	0.0|0.0| 0.0	1.7|2.5| 2.1	2.5|3.6| 3.1	2.5|3.9| 3.5	8.8|5.1| 7.1
E4	RL (Wet|Average| Dry)	0.0|0.0| 0.0	0.5|1.4| 1.5	0.8|2.1| 2.2	0.9|1.9| 2.4	6.5|6.9| 13.0
	FL (Wet|Average| Dry)	0.0|0.0| 0.2	2.2|2.8| 2.4	3.4|4.3| 4.2	3.6|4.7| 4.1	11.4|13.5| 18.3
	Total (Wet|Average| Dry)	0.0|0.0| 0.1	1.1|1.9| 1.8	1.6|2.9| 2.9	1.8|2.9|2.9	8.1|9.1| 14.8

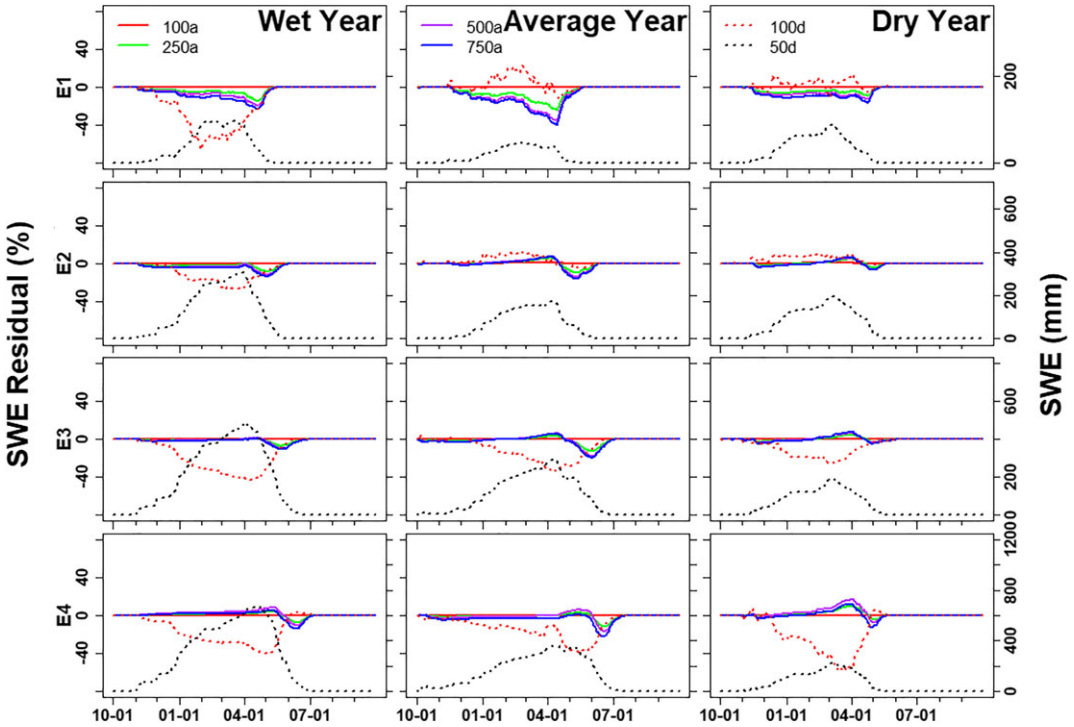

FIGURE 3 Aggregated estimated snow water equivalent (SWE) over four elevation bands. Dotted lines show the 50-m (d) and 100-m (d) scenarios, but solid lines indicate the aggregated scenarios (from the 100 (a) to 750 m (a)). Primary (left) axis shows residuals, the estimated SWE generated from all the scenarios minus that of the 50-m (d) scenario. Secondary Y (right) axis shows the estimated SWE from the 50-m (d) scenario

TABLE 4 Mean absolute error (MAE) for snow water equivalent (mm) in each band for the rising limb, falling limb, and total snow accumulation–ablation cycle

Bands	MAE (mm)	100a	250a	500a	750a	100d
E1	RL (Wet|Average| Dry)	0.1|0.0| 0.0	1.9|1.4| 2.1	2.9|2.2| 2.9	3.7|2.5| 3.8	14.4|1.7| 1.9
	FL (Wet|Average| Dry)	0.1|0.0| 0.0	3.5|2.9| 2.1	5.1|4.4| 3.3	6.3|5.0| 4.0	10.1|1.3| 2.2
	Total (Wet|Average| Dry)	0.1|0.0| 0.0	2.4|2.1| 2.1	3.5|3.2| 3.1	4.5|3.6| 3.9	13.1|1.6| 2.0
E2	RL (Wet|Average| Dry)	0.0|0.1| 0.1	3.4|1.0| 0.9	5.0|1.3| 1.2	6.3|1.2| 1.4	17.1|3.4| 4.5
	FL (Wet|Average| Dry)	0.0|0.1| 0.1	5.4|3.6| 2.3	8.0|5.2| 3.0	9.4|5.7| 3.2	13.2|1.5| 3.1
	Total (Wet|Average| Dry)	0.0|0.1| 0.1	4.0|1.7| 1.4	6.0|2.3| 1.9	7.2|2.4| 2.1	15.9|2.9| 4.0
E3	RL (Wet|Average| Dry)	0.0|0.1| 0.1	1.9|1.4| 0.8	2.1|2.2| 1.1	3.1|2.3| 1.4	45.9|11.7| 9.0
	FL (Wet|Average| Dry)	0.1|0.1| 0.1	5.4|5.9| 1.8	8.0|8.3| 2.5	8.2|9.0| 3.0	38.4|17.3| 7.1
	Total (Wet|Average| Dry)	0.1|0.1| 0.1	3.2|2.8| 1.2	4.5|4.1| 1.6	5.0|4.4| 2.0	43.1|13.5| 8.3
E4	RL (Wet|Average| Dry)	0.2|0.1| 0.0	3.1|1.7| 1.0	6.8|2.1| 2.1	4.7|5.8| 1.3	48.3|16.6| 15.4
	FL (Wet|Average| Dry)	0.2|0.2| 0.2	8.3|6.0| 4.4	13.4|9.4| 7.4	14.1|9.8| 6.0	39.4|34.5| 25.0
	Total (Wet|Average| Dry)	0.2|0.1| 0.1	4.8|3.1| 2.1	8.9|4.6| 3.9	7.7|7.1| 2.8	45.5|22.7| 18.6

elevation from E2 to E4. Residuals were negative, indicating substantial underestimation of SWE relative to the 50-m (d) simulation, except in the average and dry years in E1 and E2 when they were positive. Large residuals and MAE were observed in the wet year with an average residual of 18.8% (maximum residual of 117.2 mm) over the elevation bands. Residuals and total MAE in the average and dry years were less pronounced with an average residual of 9% (maximum residual of 64.9 mm) and 10.1% (maximum residual of 52.9 mm), respectively, relative to the wet year. Distribution of inputs at 100 m led to substantial information loss in topography-induced heterogeneity of meteorological variables as topographic features changed due to coarsening the DEM from 50 to 100 m. Loss in spatial variability of meteorological inputs caused underestimation of snow mass, particularly in the wet year and E4, where the snow mass was large.

5.2 | Causes of discrepancies in the estimated SCA and SWE?

5.2.1 | Aggregation scenarios

The differences between the 50 m (d) and the aggregated scenarios stem from the cascading effects of averaging the topography, which induces changes in topographical-sensitive meteorological inputs, to model results such as net energy fluxes. For instance, the 225 50-m cells within a 750-m area show a mosaic of ΔQ, which allows some cells to have snow cover and others to be snow free. Conversely, the 750-m (a) scenario shows only one averaged spatially homogenous energy flux for the same area, which resulted in overestimation of SCA and underestimation of SWE in E1 to E3 and overestimation of SWE in E4, during the accumulation periods (RL) and underestimation followed by overestimation of snow ablation rate in all elevation bands during the ablation period (FL).

The importance of the spatial variability of topographically sensitive meteorological data on the differences between the estimated SCA and SWE from the 50-m (d) scenario and those of the aggregated scenario is highlighted by comparing two 750-m cells, one in E2, hereafter referred as 750 m-E2-cell, and one in E4, hereafter referred as 750 m-E4-cell. These are representative cells whose behaviour is similar to others in their respective elevation bands. November 24 and October 26, 2005, were selected for the 750 m-E2-cell and 750 m-E4-cell, respectively, to show the difference in SCA and SWE during RL, and April 27 and June 20, 2006, during the ablation period.

Differences between SCA and SWE were negligible in the fall until November 20, 2009, as snow cover formed at times but ablated completely in a day or two at the 750 m-E2-cell. On November 20, snow cover formed at some 50-m cells of 50-m (d) simulation, but the cell was completely snow free for the 750-m (a) simulation at the 750 m-E2-cell, which was covered on snow on November 24, but snow still did not form in some of 50-m cells. For the 750-m (a) simulation, this caused a positive residual in SCA (Figure 4a), which became zero in the middle of December when snow cover formed at all 50-m cells within the 750 m-E2-cell. However, a negative residual in SWE remained unchanged for the rest of RL as snow accumulation and ablation rates were similar between the 750-m (a) simulation and 50-m (d) simulation at the 750 m-E2-cell.

At the 750 m-E4-cell, snow cover formed for the 750-m (a) scenario and for the 50-m (d) scenario at all 50-m cells except one on October 26, 2005 (Figure 4b). This resulted in a negligible positive residual in SCA and a large positive residual in SWE. The SWE residual increased during RL with a peak residual of 59 mm (April 26, 2006), due to underestimation of snowmelt in the 750-m (a) simulation during RL at high energy cells, similar to the cell with zero SWE on October 26, 2005 (Figure 4b).

When ablation period started, the positive residual of 59 mm in SWE for the 750-m (a) scenario increased to 60.6 mm from the prior day in the 750 m-E4-cell (Figure 5a) with a net snow cover energy flux (ΔQ) of 17.5 W/m^2. The estimated ΔQ ranged from 11.4 to 28.4 W/m^2 in the 50-m (d) scenario for 50-m cells inside the 750 m-E4-cell with average of 20.1 W/m^2 over all the 50-m cells. As a result, SWI was estimated as large as 6 mm for the 50-m cells with an average of 1.7 mm, whereas SWI of 0.1 mm was estimated for the 750-m (a) scenario for the 750 m (a)-E4-cell. This was due to neglecting energy fluxes at high energy cells. The positive residual in SWE for the 750-m (a) scenario continuously increased until snow started to melt at low energy cells. After initiation of melt at low energy cells, the positive residual decreased and eventually turned to a negative residual when snow was completely melted (zero SWE) at high energy cells. At the 750 m-E4-cell, positive residual of 1.4 mm in SWE in the 750-m (a) scenario on June 19, 2006, was turned to negative residual of 11.1 mm on June 20. On this day, SWI of 27.5 mm was estimated for the 750-m (a) scenario, whereas averaged SWI over all the 50-m

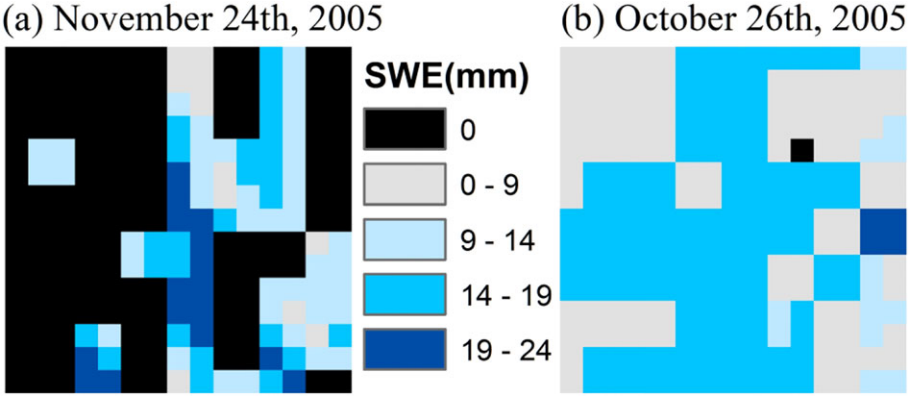

FIGURE 4 Subgrid variability of snow water equivalent (SWE) in (a) the 750 m-E2-cell and (b) 750 m-E4-cell

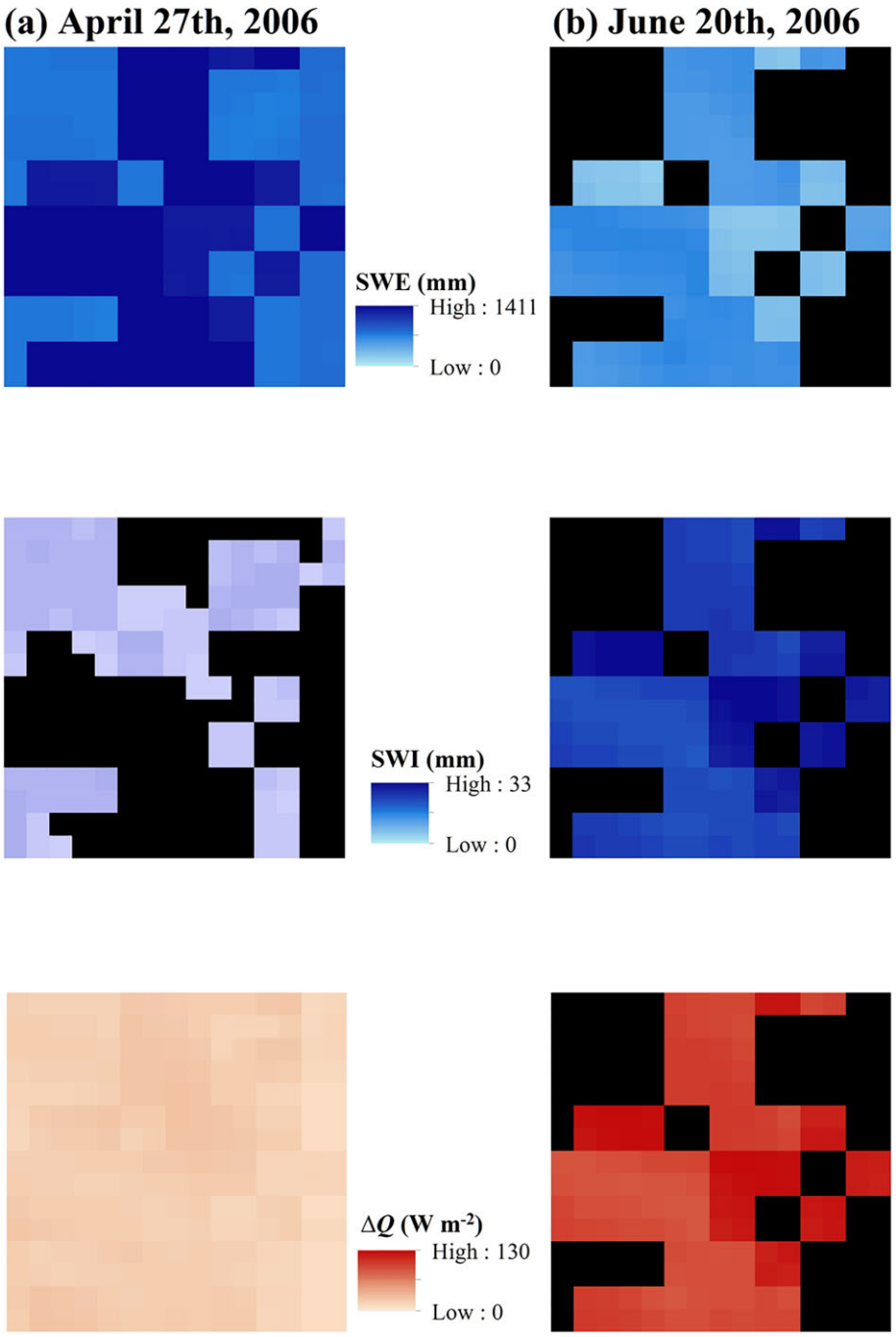

FIGURE 5 Subgrid variability of snow water equivalent (SWE), surface water input (SWI), and ΔQ in the 750 m-E4-cell

cells was 15 mm. Snow melt occurred only at low energy cells where the snow cover was still available and energy flux inputs of high energy cells had no contribution on SWE. However, energy flux inputs of high energy cells still had contribution in ablating snow in the 750-m (a) scenario, because energy flux inputs of all 50-m cells inside the 750 m-E4-cell were aggregated to generate that of the 750-m (a) scenario. This continued to the end of FL and caused FL to be shorter in the 750-m (a) scenario than in 50-m (d) scenario.

5.2.2 | Distribution scenario

Similarly to the previous section, a 100-m cell was selected in E3, hereafter 100 m-E3-cell to investigate the cascading effect of topographically sensitive meteorological inputs on estimated SCA and SWE of the 50-m (d) and 100-m (d) scenarios, on November 10, 2005, and May 20 and December 27, 2006, by coarsening the DEM from 50 to 100 m. Furthermore, to understand changes in wind-induced snow drifting due to coarsening the DEM from 50 to 100 m, *iSnobal* was run for the 100-m (d) scenario with precipitation that was distributed at 50 m and aggregated to 100 m, hereafter 100-m (d)-nodrift scenario. Addition of the 100-m (d)-nodrift scenario helps to understand how much changes in snow drifting are responsible for the differences between the estimated SCA and SWE from 50-m (d) scenario and those of the 100-m (d) scenario. The 100-m (d)-nodrift scenario was applied to the wet year *iSnobal* simulation, because this year had greater snow mass than the average and dry years.

The differences between the 50-m (d) or 100-m (a) and 100-m (d) simulations were due to changes in topographic features such as slope, aspect, sky view factor, and to some extent, elevation. Some effects of these topographic features on meteorological inputs were transferred by aggregating the inputs to obtain 100-m resolution aggregated scenario (the 100-m (a) scenario). In the 100-m (a) simulation, only variation of meteorological inputs at these four 50-m cells was lost, which had negligible impact on estimation of SCA and SWE. Even in the 750-m (a) simulation, the effects of the topographic features on meteorological inputs were transferred through the aggregation procedure. However, when inputs were distributed at 100 m, on top of overlooking variation in meteorological inputs, variations in slope, aspect, sky view factor, and elevation inside a 100-m cell were neglected. As a result, the effects of these topographic features on meteorological inputs were lost in the 100-m (d) scenario and caused significant changes in prediction of snow cover properties with substantially larger residuals of SCA and SWE than even that of the 750-m (a) simulations.

Difference between the estimated solar radiation over the 50-m (d) and 100-m (d) scenarios mainly due to changes in slope and aspect was the primary cause of observed discrepancies between these scenarios. Changes in sky view factor and to some extent elevation caused the calculated thermal radiation to be different for these scenarios. Slope changes were substantially moderated in the 100-m DEM relative to the 50-m DEM. As a result, less pronounced slope breaks were observed, which in turn resulted in moderating the effect of wind-induced snow drifting. Changes in elevation due to changing DEM resolution may lead to estimation of different relative humidity values and thus of dew point temperatures, which may cause incorrect identification of precipitation phase or inaccurate estimation of precipitation temperature and snow density.

The 50-m DEM shows a ridge where the 100 m-E3-cell is located with four 50-m cell having within 100 m-E3-cell different slopes, aspects, and elevations. This feature is not present in the 100-m DEM due to smoothing of the topography (Figure 6a). As a result of the topographical changes, estimated solar radiation in the 100-m (d) scenario was substantially larger than that of the 100-m (a) scenario during RL; this caused underestimation of snow accumulation in the 100-m (d) scenario. Solar radiation for the 100-m (d) scenario was larger in the morning than that of the 100-m (a; or 50 m (d); Figure 6d) scenario. Due to this, solar radiation for the 100-m (d) scenario was larger than that of the 100-m (a) scenario during RL when solar angle is low and sun hour in the afternoon is short. In addition, the calculated thermal radiation in the 100-m (d) scenario was larger than that of the 100-m (a) scenario (Figure 6c). During FL when sun angle is high and days are longer, solar radiation of the 100-m (d) scenario was lower than that of the 100-m (a) scenario (Figure 6f). This caused lower ablation rate in the 100-m (d) scenario relative to the 100-m (a) scenario. Similar to RL, the calculated thermal radiation in the 100-m (d) scenario was larger than that of the 100-m (a) scenario during FL (Figure 6e).

Differences in dew point temperatures of the 50-m (d) or 100-m (a) and 100-m (d) scenarios were in range of decimal degree. These small differences caused incorrect identification of precipitation phase at times when dew point temperatures fluctuated around freezing point. For instance, on December 27, 2006, precipitation occurred during the entire day and difference between precipitation phase and temperature and snow density for the 100-m (a) scenario and

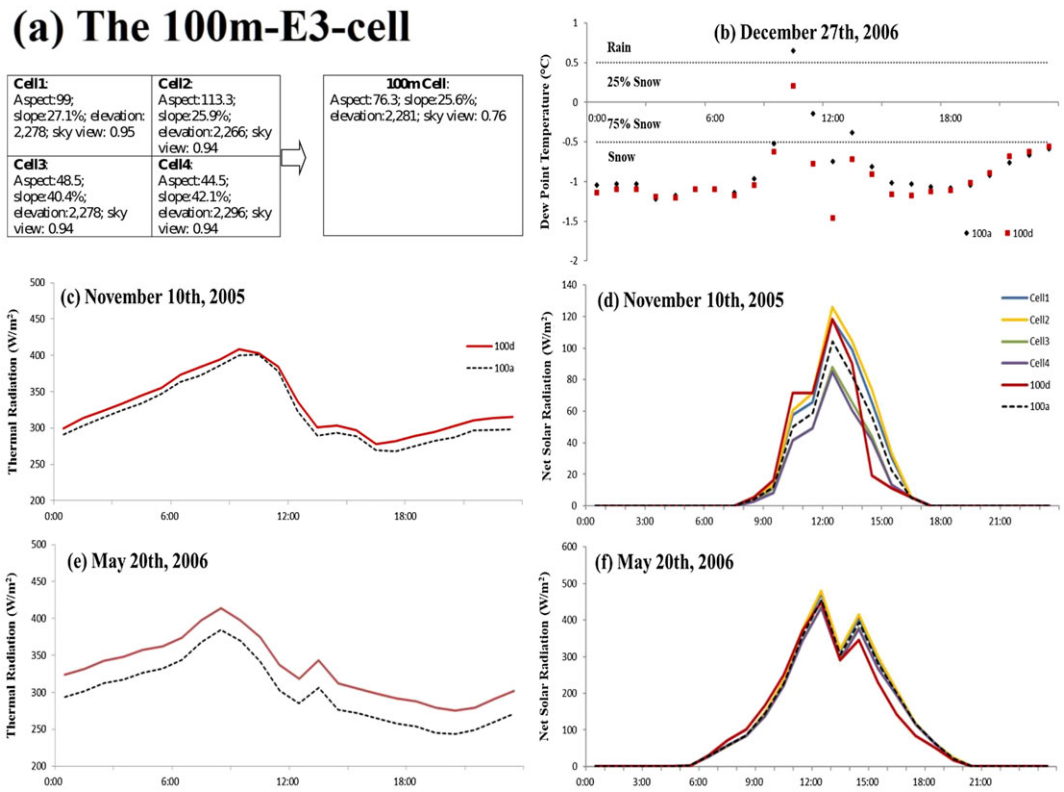

FIGURE 6 Differences in the estimated net solar and thermal radiations and dew point temperatures of the 50-m (d) or 100-m (a) scenarios and those of the 100-m (d) scenario. Panel (a) indicates that the establishment of 50-m (d) and 100-m (a) scenarios were very similar

those of the 100-m (d) scenario occurred from 10 a.m. to 1 p.m. At 10 a.m., precipitation phase was identified as a rainfall for the 100-m (a) scenario, whereas a mixed rain/snow event with 75% rain and 25% snow was estimated for the 100-m (d) scenario. Precipitation phase was estimated as snow for the 100-m (d) scenario for the rest of the day, but a mixed rain/snow event of 25% rain and 75% snow was estimated for the 100-m (a) scenario at 11 a.m. and 1 p.m. This was due to change in elevation and change in distance of grid-cell of interest from the observation sites, which were weighting factors for distributing relative humidity.

Changes in wind-induced snow drifting, which is important during RL, also affected the observed discrepancies between the 50-m (d) or 100-m (a) and 100-m (d) simulations. Extent of the discrepancies in SCA and SWE estimations caused by changes in drifting varied based on vegetation and elevation (Figure 7). SCA and SWE estimations from the 100-m (d) scenario were very similar to those of the 100-m (d)-nodrift scenario in E2, representing negligible importance of wind-induced snow drifting in this elevation band. E2 vegetation cover was coniferous forest, and in forested areas, wind-induced snow drifting is negligible (Deems et al., 2006; Trujillo et al., 2007). E1 vegetation cover was mainly sagebrush, and E3 vegetation cover was either sparse coniferous forest or bare rock. As a result, residuals in SCA and SWE during RL in the 100-m (d)-nodrift simulation were substantially lower than those of the 100-m (d) simulation in E1, E3, and E4. In SCA, the maximum residual during RL in E1 was reduced from 48.5% in the 100-m (d) simulation to 24.6% in the 100-m (d)-nodrift simulation with 4.8% reduction in MAE of RL. In E3 and E4, MAE of RL in SCA was reduced from 7.1% in the 100-m (d) simulation to 3.1% in the 100-m (d)-nodrift simulation. In SWE, MAE of RL in E3 and E4 was reduced from 48.3 mm in the 100-m (d) simulation to 37.2 mm in the 100-m (d)-nodrift simulation. In E1, MAE of RL in SWE in the 100-m (d)-nodrift simulation (7.7 mm) was about half of that of the 100-m (d) simulation (14.4 mm).

5.3 | General observation

In agreement with the results of Winstral et al. (2014), our results for the aggregated scenarios indicated negligible residuals in the 100-m (a) scenario (residuals of less than 2% in SCA and less than 0.6% in SWE)

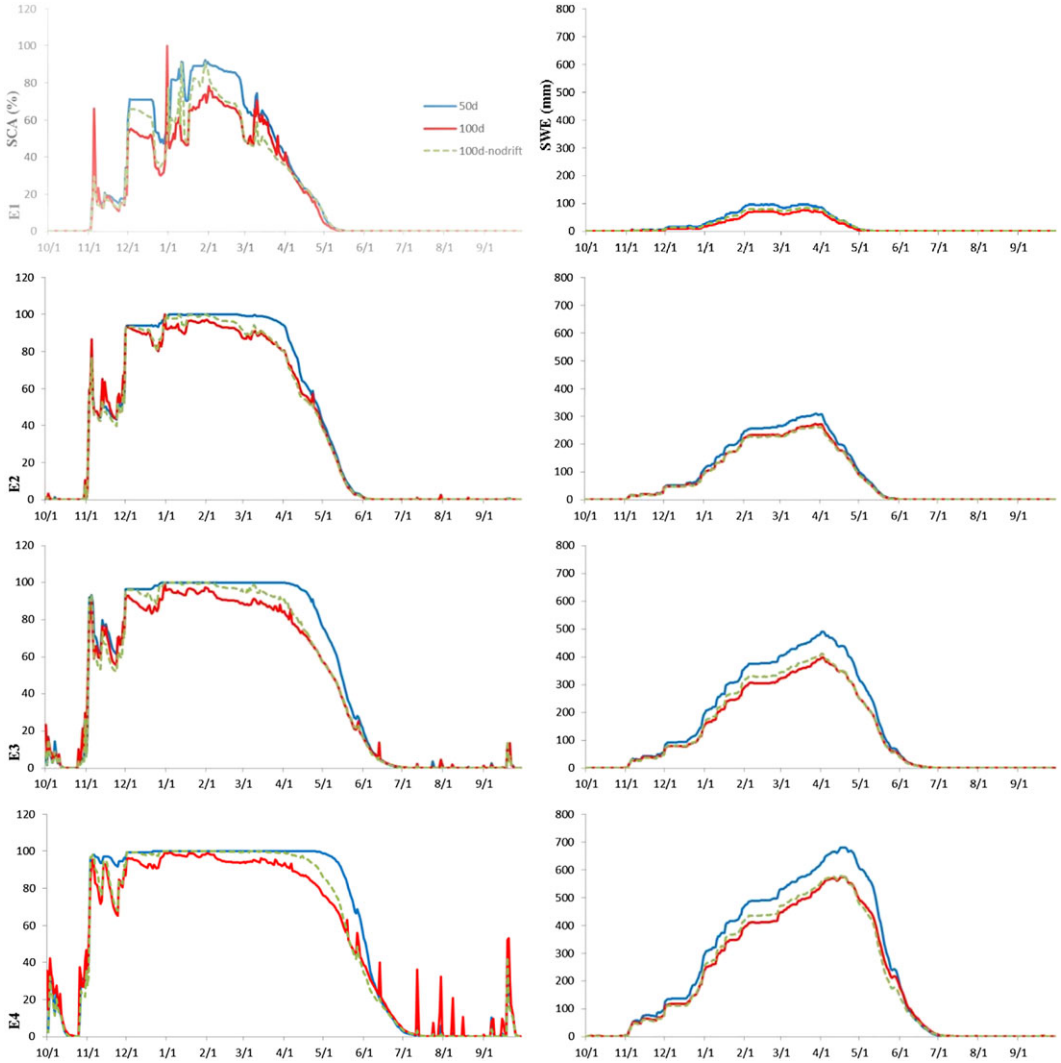

FIGURE 7 The scaling effect on the estimation of snow-covered area (SCA) and snow water equivalent (SWE) once the effect of scaling on wind-induced snow drifting was removed. The left column indicates the estimated SCA, and the right column shows the estimated SWE for the 50-m (d; solid blue line), 100-m (d; solid red line), and 100-m (d)-nodrift (dotted green line) scenarios for the wet year over the elevation bands

over all the years and elevation bands. Residuals increased as resolution coarsened. Negligible residuals were observed during accumulation period (RL), but residuals were large during FL, particularly for 500 m (a) and 750 m (a). This was due to the increase in spatial variation of energy fluxes during FL as a result of an increase in sun angle (Winstral et al., 2014). Residuals in SCA and SWE were large in the low elevation band, E1, because in this band, snow cover area is very sensitive to spatial variation in energy fluxes (Howat & Tulaczyk, 2005; Scherrer & Appenzeller, 2004). The largest differences between the estimated SCA and SWE from 50 m (d) and that of the aggregated scenarios were observed in the average year, because spatial variability of the energy fluxes might be larger in the average than the wet year due to lower humidity and fewer cloudy days (Aguado & Burt, 2013; Rohli & Vega, 2008) and precipitation volume are larger than the dry year.

This work found substantial underestimation in SCA and SWE as model spatial resolution coarsened from 50 m (50-m (d) scenario) to 100 m (100-m (d) scenario). The underestimation in SCA and SWE was caused by overestimation of solar radiation and moderating wind-induced snow drifting. Coarsening of the DEM from 50 to 100 m resulted in lower slopes, aspects, and elevations and changes in sky view factors (Kok & Ramli, 2007; Wu, Li, & Huang, 2008). This led to the overestimation of radiation input, which in turn resulted in overestimation of solar radiation and consequently overestimation of snow melt during accumulation period (Chen, Su, Ma, Yang, & Wang, 2013; Hopkinson et al., 2010). Reduction of wind-induced snow drifting was another reason for underestimation in SCA and SWE in nonforested regions, in agreement with previous works (Luce et al., 1998, 1999). Wind-induced snow drifting reduced because slopes were less steep in the 100-m DEM and less slope breaks were, thus, detected relative to the 50-m DEM (Deems et al., 2006). In contrast with Luce et al. (1998, 1999), who used a 30-m resolution DEM, this work found that topography-induced spatial variation of solar radiation is more important than spatial information of snow drifting in estimation of SCA and SWE at 50-m resolution. Snow drifting can be as important as spatial variation in solar radiation for finer than 50-m scale where slope substantially changes over small distances. SCA and SWE were overestimated in the 100-m (d) simulation relative to the 50-m (d) simulation in the average and dry years in E1 and E2. In the average and dry years, differences between recorded relative humidity at observation sites were large because spatial variation in relative humidity is greater in these years than the wet year. This was accompanied by changes in interpolation-weighting factors due to coarsening the DEM to 100 m, which caused underestimation of dew point temperatures in the 100-m (d) scenario relative to the 50-m scenario. In E1 and E2, where dew point temperatures during storms fluctuate around the freezing point during RL, underestimation of dew point temperatures even in range of decimal degree can cause misidentification of precipitation phase. As a result, snow mass was overestimated in the 100-m (d) simulation relative to the 50-m (d) simulation.

The largest residual in SCA and SWE in the 100-m (d) scenario was observed for E4, where precipitation volume was greater than other elevation bands. The largest residual in SCA occurred during the dry year, when radiation overestimation caused newly deposited snow cover to be completely ablated shortly after deposition at about 13% of cells in E4 in the 100-m (d) simulation, but SCA of 100% was estimated in the 50-m (d) simulation. The largest residual in SWE was for the wet year with an average residual of 18.8%. Precipitation mass was larger in this year than the dry and average years. As a result, solar radiation overestimation and moderating wind-induced snow drifting caused larger residuals in snow mass estimation in the 100-m (d) simulation in the wet year than the dry and average years.

These results on the effect of topo-meteorological input spatial resolution on snow modelling would be similar in any other process-based models. However, the magnitude of these effects may be different in other snow models because some models cannot provide consistently good performance for various climate conditions and vegetation and topographic settings. This is because these models do not take into account density and albedo of snow and storage of liquid water within snow (Essery, Morin, Lejeune, & Ménard, 2013), whereas *iSnobal* tracks changes in these parameters during a snow season. The elevation bands that indirectly define precipitation regimes in this work may be different in other regions depending on the latitude and regional climatology (Kormos, Marks, Williams, et al., 2014; Korner, 1998).

Whereas this study investigated the effect of climatic conditions on snow models through one wet, dry, and average year, it did not consider that different years may behave differently depending on intra-annual variability. Consequently, some processes may be more pronounced in certain years than others, but the cascading effect of topographical resolution to topographically sensitive meteorological inputs on snow processes will remain.

6 | CONCLUSION

This study explores the prediction biases of a snow melt and accumulation model introduced by the use of coarse resolution forcings and evaluates how these biases might change with different elevation ranges and climate conditions. In contrast to the prior studies on scaling of snow states, which were either limited to a short period of a snow season or small spatial extent, here, the model accuracy is evaluated vis-à-vis snow-dominated versus rain–snow transition zones and for both wet or dry periods. The evaluation was made possible by application of a spatially distributed snow model over the entire Upper Boise River Basin (Idaho, USA) with area spanning more than 6,900 km^2 and relief of 2,345 m that extends from rain-dominated elevations to snow-dominated areas above the treeline. Furthermore, instead of just using the erstwhile approach of a straightforward averaging of meteorological inputs over a coarse grid that may result in implicit transfer of information from fine resolution to those with coarse resolutions, this study explicitly accounts for the influence of coarsening of DEM on estimates of meteorological forcings and their consequent impacts on the snow model prediction biases. The investigation demonstrated that model accuracy depends not only on model scale but also on climate conditions and elevation distribution, which modulate the distribution of errors within watersheds. Our results showed that inputs of 50 m or finer resolutions are necessary because coarser resolutions lose important topography-induced spatial variation in meteorological

inputs by smoothing the topography, which has altered slope, aspect, sky view factor, and to some extent, elevation. However, the usage of finer than 250-m resolution inputs generated from aggregation of fine-scale (50 m or finer) inputs has negligible effects on prediction accuracy because information from the finer scale transfers to the aggregated model. This does not occur when data are distributed at coarser than 50-m scale. Modellers select coarse resolutions to reduce modelling costs such as runtime and storage space. Whereas the distribution of inputs on a coarse scale reduces modelling costs, the usage of coarse inputs generated from aggregating fine-scale inputs only slightly reduces modelling costs, because distributing inputs at a fine scale is the procedure that mainly increases modelling costs rather than running a snow model. Consequently fine-scale resolution topography should be used.

The smoothing effect of topography causes overestimation of solar radiation, misidentification of precipitation phase, and moderation of wind-induced snow drifting resulting in underestimation of SCA and SWE. Solar radiation is overestimated in all four elevation bands, whereas misidentification of precipitation phase occurs in rain-dominated and rain–snow transition regions, and the snow drifting effect is reduced in sparse-forested or nonforested regions like above alpine treeline. The amount of error generally increases with elevation because of two effects: (a) Low elevations are rain dominated, and (b) topographical heterogeneity increases with elevation. This suggests that finer than 50-m cell should be used at all elevations in watersheds where snow-dominated elevation bands control the hydrology.

Climatic conditions modulate the error induced by scale and elevation band. Effect of misidentification of precipitation phase on SCA and SWE estimation is noticeable in average and dry years, when spatial variability of relative humidity is high. However, the effects of solar radiation overestimation and snow drifting reduction on SCA and SWE estimation are substantially large in wet years because of large snow mass. Prediction of SCA is considerably impacted in dry years when accurate estimation of snow cover energy is necessary for snow cover retention due to a low number of precipitation events. In wet years, when snow mass is large, solar radiation overestimation and moderation of wind-induced snow drifting cause substantial underestimation of SWE. In average years, prediction of SCA is less impacted than dry years, and prediction of SWE is less affected than wet years.

ACKNOWLEDGMENTS

This study has been supported by the Bureau of Reclamation Grant RI2APJ 1025. The simulations referenced in this paper were executed on the BIG-STEM computing platform at the University of Idaho, which is supported in part by NSF Grant CNS-1229766, the Murdock Charitable Trust, and the state of Idaho's IGEM programme. Mukesh Kumar acknowledges support from NSF Grants EAR-1331846 and EAR-1454983. The authors thank Ray Anderson, director of IT at the College of Engineering of the University of Idaho, for his help with model implementation on the computing infrastructure and two anonymous reviewers for their comments and suggestions, which improved this work.

ORCID

Mohammad M. Sohrabi https://orcid.org/0000-0002-2991-1698
Daniele Tonina https://orcid.org/0000-0002-1866-1013

REFERENCES

Aguado, E., & Burt, J. E. (2013). *Understanding Weather and Climate*, Prentice Hall, p 576.

Beniston M. 2012. Is snow in the Alps receding or disappearing? WIREs Climate Change (Wiley Interdisciplinary Reviews/Climate Change) DOI:10.100

Bloschl, G. (1999). Scaling issues in snow hydrology. *Hydrological Processes*, *13*, 2149–2175. https://doi.org/10.1002/(SICI)1099-1085(199910)13:14/15<2149::AID-HYP847>3.0.CO;2-8

Blöschl, G., & Sivapalan, M. (1995). Scale issues in hydrological modelling: A review. *Hydrological Processes*, *9*(3–4), 251–290. https://doi.org/10.1002/hyp.3360090305

Chen, X., Su, Z., Ma, Y., Yang, K., & Wang, B. (2013). Estimation of surface energy fluxes under complex terrain of Mt. Qomolangma over the Tibetan Plateau. *Hydrology and Earth System Sciences*, *17*, 1607–1618. https://doi.org/10.5194/hess-17-1607-2013

Clark, M. P., Nijssen, B., Lundquist, J. D., Kavetski, D., Rupp, D. E., Woods, R. A., … Rasmussen, R. M. (2015). A unified approach for process-based hydrologic modeling: 1. Modeling concept. *Water Resources Research*, *51*(4), 2498–2514. https://doi.org/10.1002/2015WR017198

Clark, M. P., Schaefli, B., Schymanski, S. J., Samaniego, L., Luce, C. H., Jackson, B. M., … Ceola, S. (2016). Improving the theoretical underpinnings of process-based hydrologic models. *Water Resources Research*, *52*(3), 2350–2365. https://doi.org/10.1002/2015WR017910

Cristea, N. C., & Burges, S. J. (2010). An assessment of the current and future thermal regimes of three streams located in the Wenatchee River basin, Washington State: Some implications for regional river basin systems. *Climatic Change*, *102*, 493–520. https://doi.org/10.1007/s10584-009-9700-5

Darmody, R. G., Thorn, C. E., Shlyter, P., & Dixon, J. C. (2004). Relationship of vegetation distribution to soil properties in Karkevagge, swedish lapland. *Arctic, Antarctic, and Alpine Research*, *36*(1), 21–32. https://doi.org/10.1657/1523-0430(2004)036[0021:ROVDTS]2.0.CO;2

Deems, J. S., Fassnacht, S. R., & Elder, K. J. (2006). Fractal distribution of snow depth from Lidar data. *Journal of Hydrometeorology*, *7*(2), 285–297. https://doi.org/10.1175/JHM487.1

Elder, K., Dozier, J., & Michaelse, J. (1991). Snow accumulation and distribution in an alpine watershed. *Water Resources Research*, *27*(7), 1155–1541.

Essery, R., Morin, S., Lejeune, Y., & Ménard, C. B. (2013). A comparison of 1701 snow models using observations from an alpine site. *Advances in Water Resources*, *55*, 131–148. https://doi.org/10.1016/j.advwatres.2012.07.013

Garen, D. C., & Marks, D. (2005). Spatially distributed energy balance snowmelt modelling in a mountainous river basin: Estimation of meteorological inputs and verification of model results. *Journal of Hydrology*, *315*, 126–153. https://doi.org/10.1016/j.jhydrol.2005.03.026

Gu, R., McCutcheon, S., & Chen, C.-J. (1999). Development of weather-dependent flow requirements for river temperature control. *Environmental Management*, *24*(4), 529–540. https://doi.org/10.1007/s002679900252

Gupta, H. V., Sorooshian, S., & Yapo, P. O. (1998). Toward improved calibration of hydrologic models: Multiple and noncommensurable measures of information. *Water Resources Research*, *34*(4), 751–763. https://doi.org/10.1029/97WR03495

Homan, J. W., Luce, C. H., McNamara, J. P., & Glenn, N. F. (2010). Improvement of distributed snowmelt energy balance modeling with

MODIS-based NDSI-derived fractional snow-covered area data. *Hydrological Processes*, *25*, 650–660.

Hopkinson, C., Chasmer, L., Munro, S., & Demuth, M. N. (2010). The influence of DEM resolution on simulated solar radiation-induced glacier melt. *Hydrological Processes*, *24*, 775–788. https://doi.org/10.1002/hyp.7531

Howat, I. M., & Tulaczyk, S. (2005). Climate sensitivity of spring snowpack in the Sierra Nevada. *Journal of Geophysical Research*, *110*. F04021, DOI: https://doi.org/10.1029/2005JF000356

Keller, F., Goyette, S., & Beniston, M. (2005). Sensitivity analysis of snow cover to climate change scenarios and their impact on plant habitats in alpine terrain. *Climate Change*, *72*, 299–319. https://doi.org/10.1007/s10584-005-5360-2

Kirnbauer, R., Blöschl, G., & Gutknecht, D. (1994). Entering the era of distributed snow models. *Nordic Hydrology*, *25*(1–2), 1–24. https://doi.org/10.2166/nh.1994.0016

Kok, C. L., & Ramli, M. F. (2007). Scale factor and digital elevation analysis for hydrological studies. *Journal of Environmental Hydrology*, *15*, 1–12.

Kormos, P. R., Marks, D., McNamara, J. P., Marshall, H. P., Winstral, A., & Flores, A. N. (2014). Snow distribution, melt and surface water inputs to the soil in the mountain rain–snow transition zone. *Journal of Hydrology*, *519*, 190–204. https://doi.org/10.1016/j.jhydrol.2014.06.051

Kormos, P. R., Marks, D., Williams, C. J., Marshall, H. P., Aishlin, P., Chandler, D. G., & McNamara, J. P. (2014). Soil, snow, weather, and sub-surface storage data from a mountain catchment in the rain–snow transition zone. *Earth System Science Data*, *6*, 165–173. https://doi.org/10.5194/essd-6-165-2014

Korner, C. (1998). A re-assessment of high elevation treeline positions and their explanation. *Oecologia*, *115*, 445–459.

Kumar, M., Wang, R., & Link, T. E. (2012). Effects of more extreme precipitation regimes on maximum seasonal snow water equivalent. *Geophysical Research Letters*, *39*(20). https://doi.org/10.1029/2012GL052972

Link, T. E., & Marks, D. (1999). Distributed simulation of snowcover mass- and energy balance in the boreal forest. *Hydrological Processes*, *13*, 2439–2452. https://doi.org/10.1002/(SICI)1099-1085(199910)13:14/15<2439::AID-HYP866>3.0.CO;2-1

Liston, G. E. (2004). Representing subgrid snow cover heterogeneities in regional and global models. *Journal of Climate*, *17*(6), 1381–1397. https://doi.org/10.1175/1520-0442(2004)017<1381:RSSCHI>2.0.CO;2

Liston, G. E., & Elder, K. (2006). A distributed snow-evolution modeling system (SnowModel). *Journal of Hydrometeorology*, *7*(6), 1259–1276. https://doi.org/10.1175/JHM548.1

Luce, C., Staab, B., Kramer, M., Wenger, S., Isaak, D., & McConnell, C. (2014). Sensitivity of summer stream temperatures to climate variability in the Pacific Northwest. *Water Resources Research*, *50*(4), 3428–3443. https://doi.org/10.1002/2013WR014329

Luce, C. H., & Tarboton, D. G. (2004). The application of depletion curves for parameterization of subgrid variability of snow. *Hydrological Processes*, *18*, 1409–1422. https://doi.org/10.1002/hyp.1420

Luce, C. H., & Tarboton, D. G. (2010). Evaluation of alternative formulae for calculation of surface temperature in snowmelt models using frequency analysis of temperature observations. *Hydrology and Earth System Sciences*, *14*, 535–543. https://doi.org/10.5194/hess-14-535-2010

Luce, C. H., Tarboton, D. G., & Cooley, K. R. (1998). The influence of the spatial distribution of snow on basin-averaged snowmelt. *Hdrological Processes*, *12*, 1671–1683. https://doi.org/10.1002/(SICI)1099-1085(199808/09)12:10/11<1671::AID-HYP688>3.0.CO;2-N

Luce, C. H., Tarboton, D. G., & Cooley, K. R. (1999). Sub-grid parameterization of snow distribution for an energy and mass balance snow cover model. *Hydrological Processes*, *13*, 1921–1933. https://doi.org/10.1002/(SICI)1099-1085(199909)13:12/13<1921::AID-HYP867>3.0.CO;2-S

Marks, D. (1988). *Climate, energy exchange, and snowmelt in Emerald Lake watershed, Sierra Nevada*. Santa Barbara, CA: University of California.

Marks, D., Domingo, J., Susong, D., Link, T., & Garen, D. (1999). A spatially distributed energy balance snowmelt model for application in mountain basins. *Hydrological Processes*, *13*, 1935–1959. https://doi.org/10.1002/(SICI)1099-1085(199909)13:12/13<1935::AID-HYP868>3.0.CO;2-C

Marks, D., Winstral, A., Reba, M., Pomeroy, J., & Kumar, M. (2013). An evaluation of methods for determining during-storm precipitation phase and the rain/snow transition elevation at the surface in a mountain basin. *Journal of Advances in Water Resources*, *55*, 98–110. https://doi.org/10.1016/j.advwatres.2012.11.012

Meromy, L., Molotch, N. P., Link, T. E., Fassnacht, S. R., & Rice, R. (2013). Subgrid variability of snow water equivalent at operational snow stations in the western USA. *Hydrological Processes*, *27*, 2383–2400. https://doi.org/10.1002/hyp.9355

Mizukami, N., Clark, M. P., Slater, A. G., Brekke, L. D., Elsner, M. M., Arnold, J. R., & Gangopadhyay, S. (2014). Hydrologic implications of different large-scale meteorological model forcing datasets in mountainous regions. *Journal of Hydrometeorology*, *15*(1), 474–488. https://doi.org/10.1175/JHM-D-13-036.1

Molotch, N. P., & Bales, R. C. (2005). Scaling snow observations from the point to the grid element: Implications for observation network design. *Water Resources Research*, *41*. W11421, DOI: https://doi.org/10.1029/2005WR004229

Moriasi, D. N., Arnold, J. G., Van, L. M. W., Bingner, R. L., Harmel, R. D., & Veith, T. L. (2007). Model evaluation guidelines for systematic quantification of accuracy in watershed simulations. *Transactions of the ASABE*, *50*(3), 885–900. https://doi.org/10.13031/2013.23153

Nitaa, T., Yoshimura, K., Takata, K., O'ishi, R., Sueyoshi, T., Kanae, S., … Liston, G. E. (2014). Representing variability in subgrid snow cover and snow depth in a global land model: Offline validation. *Journal of Climate*, *27*, 3318–3330. https://doi.org/10.1175/JCLI-D-13-00310.1

Niu, G.-Y., & Yang, Z.-L. (2007). An observation-based formulation of snow cover fraction and its evaluation over large North American river basins. *Journal of Geophysical Research*, *112*. D21101, https://doi.org/10.1029/2007JD008674

Pohl, S., & Marsh, P. (2006). Modelling the spatial–temporal variability of spring snowmelt in an arctic catchment. *Hydrological Processes*, *20*, 1773–1792. https://doi.org/10.1002/hyp.5955

Pohl, S., Marsh, P., & Liston, G. E. (2006). Spatial-temporal variability in turbulent fluxes during spring snomelt. *Arctic, Antarctic, and Alpine Research*, *38*(1), 136–146. https://doi.org/10.1657/1523-0430(2006)038[0136:SVITFD]2.0.CO;2

Raleigh, M. S., & Lundquist, J. D. (2012). Comparing and combining SWE estimates from the SNOW-17 model using PRISM and SWE reconstruction. *Water Resources Management*, *48*. W01506

Rohli, R. V., & Vega, A. J. (2008). The climate system: Controls on climate. In *Climotology* (pp. 30–60). Jones and Bartlett Publishers.

Scherrer, S. C., & Appenzeller, C. (2004). Trends in Swiss Alpine snow days: The role of local- and large-scale climate variability. *Geophysical Research Letters*, *31*. L13215, DOI: https://doi.org/10.1029/2004GL020255

Schimel, J. P., Bilbrough, C., & Welker, J. M. (2004). Increased snow depth affects microbial activity and nitrogen mineralization in two Arctic tundra communities. *Soil Biology & Biochemistry*, *36*, 217–227. https://doi.org/10.1016/j.soilbio.2003.09.008

Sensoy, A., Sorman, A. A., Tekeli, A. E., Sorman, A. U., & Garen, D. C. (2006). Point-scale energy and mass balance snowpack simulations in the upper Karasu basin, Turkey. *Hydrological Processes*, *20*, 899–922. https://doi.org/10.1002/hyp.6120

Seyednasrollah, B., & Kumar, M. (2014). Net radiation in a snow-covered discontinuous forest gap for a range of gap sizes and topographic configurations. *Journal of Geophysical Research-Atmospheres*, *119*(17), 10323–10342. https://doi.org/10.1002/2014JD021809

Seyednasrollah, B., Kumar, M., & Link, T. E. (2013). On the role of vegetation density on net snow cover radiation at the forest floor. *Journal of Geophysical Research-Atmospheres*, *118*(15), 8359–8374. https://doi.org/10.1002/jgrd.50575

Sohrabi, M. M. (2016). *Lost and transferred information by changing spatial and temporal resolution in hydrological modeling*. University of Idaho, ProQuest Dissertations Publishing.

Sohrabi, M. M., Benjankar, R., Tonina, D., Kumar, M., Marks, D., & Kormos, P. (2018). Role of temporal resolution of meteorological inputs for process-based snow modeling. *Hydrological Processes*, *32*, 1–14. https://doi.org/10.1002/hyp.13242

Sohrabi, M. M., Benjankar, R., Tonina, D., Wenger, S. J., & Isaak, D. J. (2017). Estimation of daily stream water temperatures with a Bayesian regression approach. *Hydrological Processes*, *31*(9), 1719–1733.

Sohrabi, M. M., Ryu, J., Abatzoglou, J., & Tracy, J. (2013). Climate extreme and its linkage to regional drought over Idaho. *Natural Hazards*, *65*(1), 653–681. https://doi.org/10.1007/s11069-012-0384-1

Sohrabi, M. M., Ryu, J., Abatzoglou, J., & Tracy, J. (2015). Development of soil moisture drought index to characterize droughts. *Journal of Hydrologic Engineering*, *20*(11), 4015025. https://doi.org/10.1061/(ASCE)HE.1943-5584.0001213

Sturm, M., Holmgren, J., König, M., & Morris, K. (1997). The thermal conductivity of seasonal snow. *Journal of Glaciology*, *43*, 26–41. https://doi.org/10.1017/S0022143000002781

Susong, D., Marks, D., & Garen, D. C. (1999). Methods for developing time-series climate surfaces to drive topographically distributed energy- and water-balance models. *Hydrological Procedure*, *13*, 2003–2021. https://doi.org/10.1002/(SICI)1099-1085(199909)13:12/13<2003::AID-HYP884>3.0.CO;2-K

Tarboton, D., Blöschl, G., Cooley, K., Kirnbauer, R., & Luce, C. (2001). Spatial snow cover processes at Kühtai and Reynolds Creek. In R. Grayson, & G. Blöschl (Eds.), *Spatial Patterns in Catchment Hydrology: Observations and Modelling* (pp. 158–186). Cambridge: Cambridge University Press.

Tobin, K. J., & Bennett, M. E. (2017). Constraining SWAT calibration with remotely sensed evapotranspiration data. *Journal of the American Water Resources Association*, *53*(3), 593–604. https://doi.org/10.1111/1752-1688.12516

Torp, M. (2010). *The effect of snow on plants and their interactions with herbivores*. Umeå: Umeå University.

Trujillo, E., Rami'rez, J. A., & Elder, K. J. (2007). Topographic, meteorologic, and canopy controls on the scaling characteristics of the spatial distribution of snow depth fields. *Water Resources Research*, *43*. W07409, DOI: https://doi.org/10.1029/2006WR005317

Wang, R., Kumar, M., & Marks, D. (2013). Anomalous trend in soil evaporation in a semi-arid, snow-dominated watershed. *Advances in Water Resources*, *57*, 32–40. https://doi.org/10.1016/j.advwatres.2013.03.004

Webb, B. W., Clack, P. D., & Walling, D. E. (2003). Water–air temperature relationships in a Devon river system and the role of flow. *Hydrological Processes*, *17*, 3069–3084. https://doi.org/10.1002/hyp.1280

Weill, S., Altissimo, M., Cassiani, G., Deiana, R., Marani, M., & Putti, M. (2013). Saturated area dynamics and streamflow generation from coupled surface–subsurface simulations and field observations. *Advances in Water Resources*, *59*, 196–208. https://doi.org/10.1016/j.advwatres.2013.06.007

Winstral, A., Elder, K., & Davis, R. E. (2002). Spatial snow modeling of wind-redistributed snow using terrain-based parameters. *Journal of Hydrometeorology*, *3*, 524–538. https://doi.org/10.1175/1525-7541(2002)003<0524:SSMOWR>2.0.CO;2

Winstral, A., & Marks, D. (2002). Simulating wind fields and snow redistribution using terrain-based parameters to model snow accumulation and melt over a semi-arid mountain catchment. *Hydrological Processes*, *16*, 3585–3603. https://doi.org/10.1002/hyp.1238

Winstral, A., Marks, D., & Gurney, R. (2009). An efficient method for distributing wind speeds over heterogeneous terrain. *Hydrological Processes*, *23*, 2526–2535. https://doi.org/10.1002/hyp.7141

Winstral, A., Marks, D., & Gurney, R. (2013). Simulating wind-affected snow accumulations at catchment to basin scales. *Advances in Water Resources*, *55*, 64–79. https://doi.org/10.1016/j.advwatres.2012.08.011

Winstral, A., Marks, D., & Gurney, R. (2014). Assessing the sensitivities of a distributed snow model to forcing data resolution. *Journal of Hydrometeorology*, *15*, 1366–1383. https://doi.org/10.1175/JHM-D-13-0169.1

Wu, S., Li, J., & Huang, G. H. (2008). A study on DEM-derived primary topographic attributes for hydrologic applications: Sensitivity to elevation data resolution. *Applied Geography*, *28*(3), 210–223. https://doi.org/10.1016/j.apgeog.2008.02.006

How to cite this article: Sohrabi MM, Tonina D, Benjankar R, et al. On the role of spatial resolution on snow estimates using a process-based snow model across a range of climatology and elevation. *Hydrological Processes*. 2019;33:1260–1275. https://doi.org/10.1002/hyp.13397